

1 **BrGDGTs-based seasonal paleotemperature reconstruction for the last 15,000 years from**
2 **a shallow lake on the eastern Tibetan Plateau**

3 Xiaohuan Hou ^a, Nannan Wang ^a, Zhe Sun ^b, Kan Yuan ^{a, c}, Xianyong Cao ^a, Juzhi Hou ^{a *}

4 ^a *Group of Alpine Paleoecology and Human Adaptation (ALPHA), State Key Laboratory of Tibetan*
5 *Plateau Earth System, Resources and Environment (TPESRE), Institute of Tibetan Plateau Research,*
6 *Chinese Academy of Sciences, Beijing 100101, China*

7 ^b *Institute of Geography and Resources Science, Sichuan Normal University, Chengdu, 610066, China*

8 ^c *University of Chinese Academy of Sciences, Beijing 100049, China*

9

10 * Corresponding author

11 E-mail address: houjz@itpcas.ac.cn

12

13 **ABSTRACT**

14 Understanding Holocene temperature changes is vital for resolving discrepancies between
15 proxy reconstructions and climate models. The intricate temperature variations across the
16 Tibetan Plateau (TP) add complexity to studying continental climate change during this
17 period. Discrepancies between model-based and proxy-based reconstructions might stem
18 from seasonal biases and environmental uncertainties in the proxies. Employing multiple
19 proxies from a single sediment core for quantitative temperature reconstructions offers an
20 effective method for cross-validation in terrestrial environments. Here, we present an ice-
21 free-season temperature record for the past 15 ka from a shallow, freshwater lake on the
22 eastern TP, based on brGDGTs (branched glycerol dialkyl glycerol tetraethers). This record
23 shows that the Holocene Thermal Maximum lags the pollen-based July temperature recorded
24 in the same sediment core. We conclude that the mismatch between the brGDGTs-based and
25 pollen-based temperatures is primarily the result of seasonal variations in solar irradiance.
26 The overall pattern of temperature changes is supported by other summer temperature
27 records, and the Younger Dryas cold event and the Bølling–Allerød warm period are also
28 detected. A generally warm period occurred during 8–3.5 ka, followed by a cooling trend in
29 the late Holocene. Our findings have implications for understanding the seasonal signal of
30 brGDGTs in shallow lakes, and provide critical data for confirming the occurrence of
31 seasonal biases in different proxies from high-elevation lakes. To further investigate the
32 significance of the brGDGTs and temperature patterns on the TP, we examined existing
33 brGDGTs-based Holocene temperature records, which interpret these compounds as
34 indicators of mean annual or growing season temperatures. The existing/available

35 temperature records show complicated patterns of variation, some with general warming
36 trends throughout the Holocene, some with cooling trends, while some with warm middle
37 Holocene. We analyzed the possible reasons for the diverse brGDGTs records on the TP and
38 emphasize the importance of considering lake conditions and modern investigations of
39 brGDGTs in lacustrine systems when using brGDGTs to reconstruct paleoenvironmental
40 conditions.

41 **Keywords:** Tibetan Plateau, brGDGTs, the mean temperature of Months Above Freezing,
42 shallow lake, Holocene

43 **1 Introduction**

44 Global climate change has a profound impact on both the natural ecological and socio-
45 economic systems that are vital for human survival and development, making climate change
46 a critical limiting factor for the sustainable development of human society. The Tibetan Plateau
47 (TP), also called the “Third Pole” (Qiu, 2008), has undergone a more rapid warming over the
48 last five decades, with a rate twice that of the global average ($0.3 - 0.4^{\circ}\text{C}/\text{decade}$) (Kuang and
49 Jiao, 2016; Chen et al., 2015), making it one of the world's most temperature-sensitive regions
50 (Chen et al., 2015; Yao et al., 2022). Consequently, assessing the impact of future climate
51 change on the TP is becoming increasingly important. To enhance the precision and accuracy
52 of future climate change estimates for the TP under ongoing global climate change and to
53 minimize the uncertainty in climate simulations, it is essential to investigate the processes and
54 mechanisms of regional climate and environmental changes, with particular emphasis on
55 temperature, on a relatively long timescale, such as that of the Holocene.

56

57 The Holocene, the most recent geological epoch, is closely linked with the development of
58 human civilization. Quantitative reconstructions of Holocene temperature trends can be used
59 to explore their impacts on civilization and to establish a geological and historical context for
60 predicting future climate changes. In recent decades, many Holocene quantitative
61 reconstructions of seasonal and annual temperatures for the TP have been produced using
62 various proxies, like pollen (Herzschuh et al., 2014; Lu et al., 2011), chironomids (Zhang et al.,
63 2017; Zhang et al., 2019a), $\delta^{18}\text{O}$ in ice cores (Pang et al., 2020; Thompson et al., 1997), and
64 biomarkers (Hou et al., 2016; Zhao et al., 2013; Cheung et al., 2017). These reconstructions
65 have provided crucial data for the elucidation of Holocene temperature changes. However, the
66 available Holocene temperature records from the TP show divergent trends. Multiple proxy
67 indicators indicate three different Holocene temperature patterns on the TP. First, a consistent
68 Holocene warming trend (Sun et al., 2022; Feng et al., 2022; Opitz et al., 2015). For example,
69 brGDGTs based annual temperatures (Feng et al., 2022; Sun et al., 2022) indicate a gradual
70 warming trend which resembles the $\delta^{18}\text{O}$ temperature record from the Chongce ice core on the
71 western TP, except for the last 2 ka (Pang et al., 2020). Second, an early to middle Holocene
72 summer temperature maximum and a gradual cooling trend during the late Holocene are
73 observed in pollen-, alkenone- and chironomid-based temperature records (Herzschuh et al.,
74 2014; Hou et al., 2016; Zhang et al., 2017; Wang et al., 2021a; Zheng et al., 2015). Third, a
75 prominent relatively cool middle Holocene (Wang et al., 2021c; Li et al., 2017); for example,
76 a composite temperature record suggests that temperatures were $\sim 2^\circ\text{C}$ cooler during the middle
77 Holocene than during the early and late Holocene (Wang et al., 2021c). Several records also
78 show a steady long-term trend without distinct cooling or warming (Sun et al., 2021). Moreover,

79 the cooling trends in proxy-based Holocene temperature records are inconsistent with those of
80 climate models, which indicate a warming trend, and this inconsistency is widely known as the
81 “Holocene temperature conundrum” (Liu et al., 2014). There are several potential factors that
82 may contribute to the disparity in Holocene temperature trends, including seasonal biases and
83 uncertainties in temperature proxies and reconstructions, independent of climate models (Liu
84 et al., 2014; Hou et al., 2019; Bova et al., 2021; Cartapanis et al., 2022; Marsicek et al., 2018).
85 While several recent studies have suggested that seasonality in proxies is not the major cause
86 of the Holocene temperature conundrum (Dong et al., 2022; Zhang et al., 2022b), it is
87 significant that the TP is an alpine and high-altitude region with significant seasonal
88 temperature variations. Moreover, most organisms tend to grow during the warmer seasons at
89 high latitudes and high altitudes (Zhao et al., 2021a). Currently, however, we lack unambiguous
90 and reliable seasonal temperature records to support a seasonality-bias hypothesis. Extensive
91 research has been conducted in lakes, employing a single proxy to reconstruct past temperature
92 fluctuations. However, there have been scarce studies that employ various proxies within the
93 same core to reconstruct paleotemperature variations. Furthermore, the limited number of
94 studies primarily concentrate on reconstructing summer temperature and annual average
95 temperature. For example, a chironomid-based July temperature reconstruction for Tiancai lake
96 on the southeastern TP shows higher temperatures during the early to middle Holocene (Zhang
97 et al., 2017), while the brGDGTs-based annual average temperature shows a warming trend
98 (Feng et al., 2022). Different proxies may reflect the seasonal temperatures in different months,
99 and thus producing temperature reconstructions for different months for the same sediment
100 core may help better understand the seasonal bias of terrestrial temperature records.

101 Furthermore, the reconciliation of the divergent trends of Holocene temperature on the TP and
102 its surroundings requires additional high-altitude temperature records from these regions, with
103 reliable chronologies and proxy records with an unambiguous climatological significance.

104

105 Branched glycerol dialkyl glycerol tetraethers (brGDGTs) are a group of membrane-spanning
106 lipids found in bacteria (Fig. S1) (Chen et al., 2022; Halamka et al., 2022; Sinninghe Damsté
107 et al., 2000), and they have become a powerful tool for quantifying past terrestrial temperature
108 variations. Through investigations of brGDGTs in globally-distributed soils, it was found that
109 the distribution of brGDGTs is primarily related to temperature and pH (Weijers et al., 2007).
110 Subsequently, brGDGTs–temperature calibrations from soil, peat and lake sediments were
111 established on scales from global (Weijers et al., 2007; De Jonge et al., 2014; Crampton-Flood
112 et al., 2020; Martínez-Sosa et al., 2021) to regional (e.g., East Asia) (Sun et al., 2011; Ding et
113 al., 2015; Wang et al., 2016; Dang et al., 2018), leading to considerable progress in
114 reconstructing terrestrial temperatures, particularly on the TP (Cheung et al., 2017; Zhang et
115 al., 2022a; Li et al., 2017).

116

117 Natural lakes are widely distributed across the TP (Zhang et al., 2019b). Lake sediments,
118 characterized by their organic matter-rich composition, exhibit continuous and rapid
119 accumulation rates. As a result, they offer high-resolution records of environmental changes,
120 making them highly valued as a primary terrestrial climate archive (Moser et al., 2019).
121 BrGDGTs in lacustrine systems are often more strongly correlated with temperature, with
122 higher coefficient of determination (r^2) and lower root mean square error (RMSE) values

123 (Martínez-Sosa et al., 2021), than in soils and peats. Nevertheless, the factors that impact the
124 distribution of brGDGTs in lakes are intricate and multidimensional. Notably, the sources of
125 brGDGTs within lakes are intricate, involving contributions from soil as well as autochthonous
126 lake processes. However, an expanding body of research underscores a substantial prevalence
127 of autochthonous brGDGTs in lakes (Tierney and Russell, 2009; Tierney et al., 2010; Weber et
128 al., 2015; Wang et al., 2021b). Furthermore, the origins of brGDGT producers remain uncertain
129 and could be influenced by various factors, including lake salinity (Wang et al., 2021b), redox
130 conditions (Weber et al., 2018), oxygen content and/or mixing patterns (Van Bree et al., 2020;
131 Wu et al., 2021; Buckles et al., 2014). Additionally, even lake depth plays a role due to distinct
132 ecological niches (Woltering et al., 2012), thereby contributing to the intricate interplay that
133 shapes the distribution of brGDGTs within lakes.

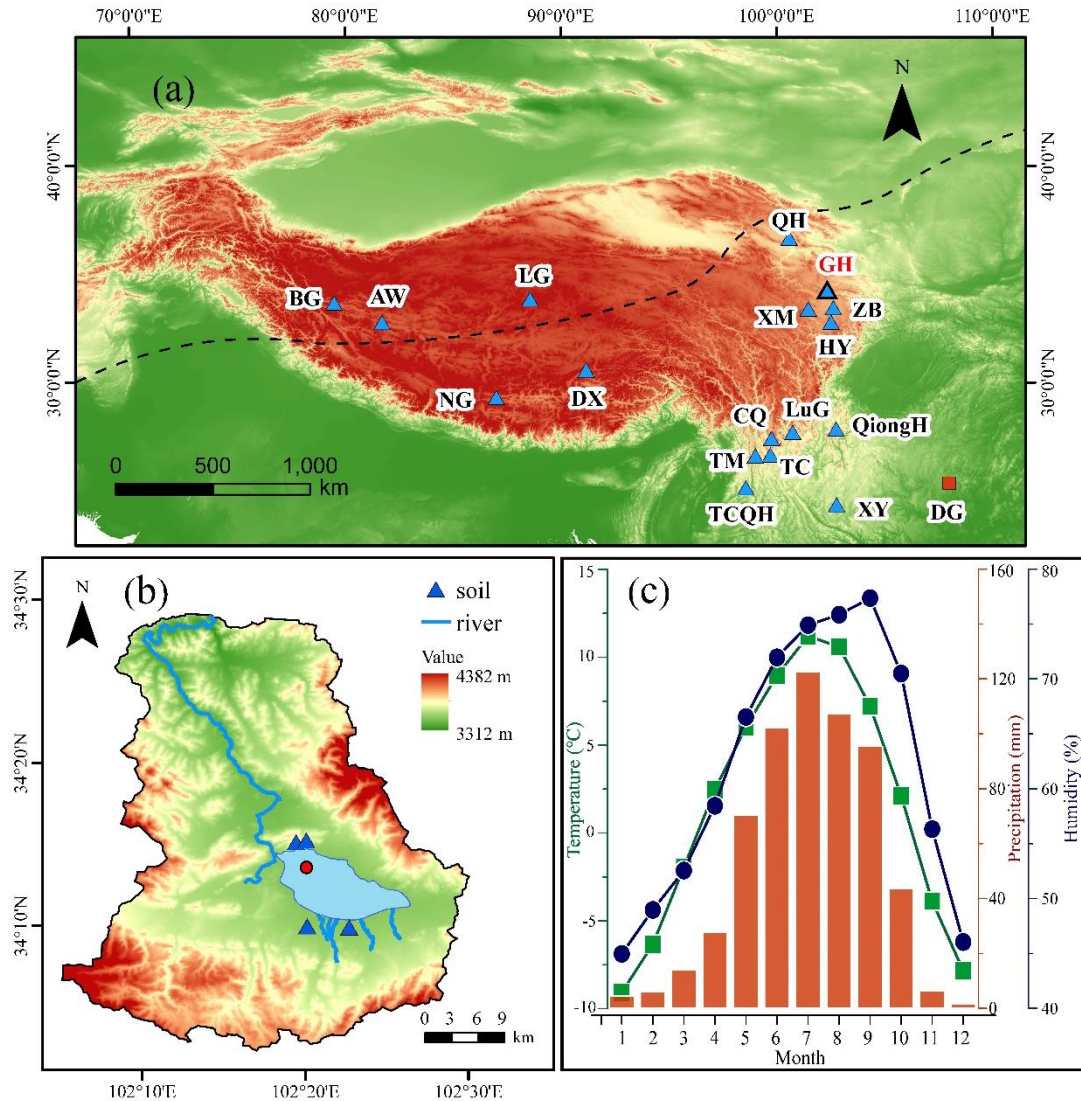
134

135 In this study, we obtained a quantitative temperature reconstruction for the past 15 ka from
136 Gahai, a shallow (average depth of ~2 m) freshwater lake located in the source area of the
137 Yellow River. This region is an important ecological protection area on the eastern edge of the
138 TP. Freshwater environments avoid the confounding effects of salinity on brGDGTs-based
139 temperature reconstructions, and shallow lakes also minimize the impact of the uneven
140 distribution of light and nutrients on brGDGTs. Our specific aims were: (1) to determine the
141 long-term trend of Holocene warm-biased terrestrial temperatures at a high elevation; (2) to
142 compare records of ice-free season temperatures with July temperatures from the same
143 sediment core; and (3) to gain a better understanding of the possible mechanisms responsible
144 for Holocene temperature variations, especially on the TP.

145 **2 Materials and methods**

146 *2.1 Study site*

147 Gahai (102°11'–102°28' E, 34°04'–34°4' N, 3444 m a.s.l.) is a freshwater lake and part of the
148 Gahai meadow wetland, which is a national nature reserve with restricted human access, on the
149 eastern edge of the Tibetan Plateau (Fig. 1). The lake is fed by runoff from the surrounding
150 hills, drains into the Tao River, and ultimately enters the Yellow River. Thus, Gahai lake is a
151 critical water conservation area in the upper reaches of the Yellow River. The average water
152 depth of Gahai is ~1–2 m, and the maximum depth is ~5 m. The vegetation in the catchment
153 consists mainly of *Kobresia tibetica*, *Equisetum arvense*, *Potentilla anserina*, *Artemisia*
154 *subulate*, and *Oxytropis falcata* (Ma et al., 2019). Meteorological data for the area are available
155 from Langmu Temple station (1957-1988) (Fig. 1) (102°38' E, 34°5' N, 3412 m a.s.l.), ~32 km
156 northwest of Gahai lake. They indicate an annual average (mean) precipitation of 781 mm,
157 with > 67% occurring between June and September, and mean annual temperature of 1.2 °C
158 with a relative humidity of ~65%. The summers are mild and humid and the winters are cold
159 and dry. From May to September, the mean average temperature is above freezing (0°C), but
160 the temperature in May is very low, close to 0°C.



161

162 **Fig. 1** (a) Locations of the sites on the Tibetan Plateau referenced in the text. Triangle with
 163 bold line indicates the location of Gahai lake (this study). Other triangles indicate the
 164 locations of cited studies on the Tibetan Plateau and the surrounding area: Bangong Co
 165 (BG), Aweng Co (AW), Ngamring Co (NG), Linggo Co (LG), Dangxiong wetland (DX),
 166 Qinghai lake (QH), Ximen Co (XM), Zoige Basin (ZB), Hongyuan peatland (HY), Lugu
 167 lake (LuG), Cuoqia lake (CQ), Tingming lake (TM), Tengchongqinghai lake (TCQH),
 168 Tiancai lake (TC), Qionghai lake (QH), Xingyun lake (XY). Red square indicates
 169 Dongge Cave (DG). Black dotted line represents the northern boundary of the modern
 170 Asian summer Monsoon (Chen et al., 2008). (b) Drainage basin of Gahai lake and the
 171 core site. (c) Climate data from Langmu Temple meteorological station: monthly
 172 temperature (green line), precipitation (red bars), and humidity (blue line).

173 *2.2 Sampling*

174 A sediment core with the length of 329 cm was obtained from Gahai Lake in January 2019, at
175 a water depth of 1.95 m, using a UWITEC platform operated from the frozen lake surface. In
176 addition, four catchment soil samples were collected from around the lake (Fig. 1). All samples
177 were transported to the Institute of Tibetan Plateau Research, Chinese Academy of Sciences
178 (ITPCAS). The sediment core was split lengthwise, and one half was subsampled and freeze-
179 dried for subsequent analysis.

180

181 *2.3 Chronology*

182 The chronology of the upper 20 cm of the sediment core is based on measurements of ^{210}Pb
183 and ^{137}Cs , at a 1-cm interval. The chronology for the deeper part of the core is provided by
184 accelerator mass spectrometry (AMS) ^{14}C measurements of 13 bulk sediment samples, which
185 were conducted by Beta Analytic Inc. (Miami, USA) (Fig. 2) (Wang et al., 2022).

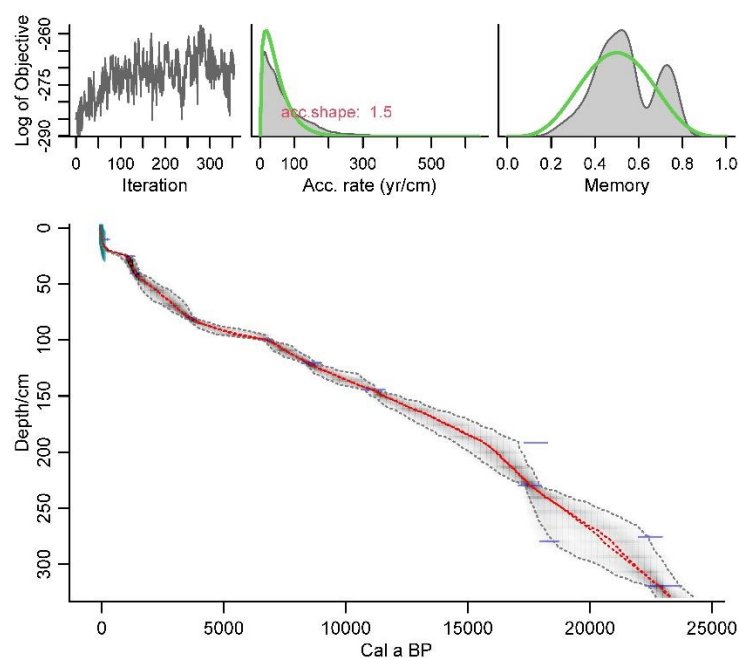
186

187 The ^{210}Pb age model was constructed using the constant rate of supply (CRS) model and the
188 ^{137}Cs peak was used as supplement (Appleby, 2002). The calculated age of ^{210}Pb using CRS
189 model aligned well with the ^{137}Cs peak at 6 cm. Overall, the CRS model was deemed suitable
190 for determining the age of Gahai lake.

191

192 Reservoir age, as highlighted by Hou et al. (2012), is a crucial factor affecting the age
193 determination of lake sediment cores on the TP. Therefore, it was necessary to establish the
194 reservoir age of Gahai lake before undertaking paleoclimate reconstruction. The linear

195 extrapolation relationship between the ^{14}C ages and depth to the sediment-water interface is
196 often used to estimate the reservoir age. The ^{14}C age of 13 samples exhibits a good linear
197 relationship with sediments depth in Gahai lake. Extrapolation of this 13 ^{14}C ages down to the
198 depth of 6 cm yielded a ^{14}C age of 461 yr BP, while the reliable ^{210}Pb age at 6 cm is -27 yr BP.
199 Consequently, the difference between the two ages, which amounts to 488 yr, was taken as the
200 reservoir age. Additionally, it's worth noting that independent estimations of the ^{14}C calibration
201 age and ^{210}Pb age around 10 cm in Gahai lake was obtained, resulting in values of 497 yr BP
202 and 18 yr BP, respectively. The difference of 479 yr between these two ages can also be
203 considered as the reservoir age. These two methods of estimating reservoir age of Gahai lake
204 show very close, which are mutually supportive. So, the average of 483 yr was adopted as the
205 reservoir age. All original ^{14}C dates were corrected by subtracting the reservoir age (483 yr)
206 and calibrating them to calendar ages using Calib 8.1. The age-depth model (Fig. 2) was
207 constructed using the Bacon program with the ^{14}C ages and ^{210}Pb ages (Blaauw and Andres
208 Christen, 2011) and was reported by Wang et al. (2022).



209

210 **Fig. 2** Age-depth model for Gahai, based on AMS ^{14}C , ^{210}Pb and ^{137}Cs ages (Wang et al.,
211 2022). The ages of the upper 20 cm are based on ^{210}Pb and ^{137}Cs dating (green symbols)
212 and those of the lower part on AMS ^{14}C dates (blue symbols).

213

214 *2.4 Lipids extraction and brGDGTs analysis*

215 For lipids extraction, ~5 g samples were ground to a powder and extracted ultrasonically with
216 dichloromethane (DCM): methanol (MeOH) (9: 1, v: v) three times. The supernatants were
217 combined and dried under a stream of nitrogen gas. Subsequently, the total lipid extracts were
218 separated into neutral and acid fractions through a LC-NH₂ silica gel column using DCM:
219 isopropyl alcohol (2: 1, v: v) and ether with 4% acetic acid (v: v), respectively. The neutral
220 fraction was then eluted through a silica gel column using n-Hexane, DCM and MeOH, and
221 the GDGTs were dissolved in the MeOH. The GDGTs fraction was passed through a 0.45 μm
222 polytetrafluoroethylene (PTFE) filter before analysis. C₄₆-GDGT (a standard compound)
223 (Huguet et al., 2006) was added to the samples before analysis.

224

225 BrGDGTs were detected using an HPLC-APCI-MS (Waters ACQUITY UPLC I-Class/Xevo
226 TQD) with auto-injection at the ITPCAS. The compounds were separated by three Hypersil
227 Gold Silica LC columns in sequence (each 100 mm \times 2.1 mm, 1.9 μm , Thermo Fisher Scientific;
228 USA), maintained at a temperature of 40°C. GDGTs were eluted isocratically using 84%
229 hexane and 16% ethyl acetate (EtOA) for the first 5 min, followed by a linear gradient change
230 to 82% hexane and 18% EtOA from 5 to 65 min. The columns were cleaned using 100% EtOA
231 for 10 min, and then back to 84% hexane and 16% EtOA to equilibrate the column, with a flow
232 rate of 0.2 ml min⁻¹.

233

234 The APCI-MS conditions were as follows: nebulizer pressure at 60 psi, APCI probe
235 temperature at 400°C, drying gas flow rate of 6 L/min and temperature of 200°C, capillary
236 voltage of 3600 V, source corona of 5.5 μ A. Detection was performed in selected ion
237 monitoring (SIM) mode, targeting the protonated molecules at m/z 1050, 1048, 1046, 1036,
238 1034, 1032, 1022, 1020, 1018 and 744. The results were analyzed using MassLynx V4.1
239 software, and quantification was achieved by comparing the peak areas of targeted ions and the
240 internal standard, assuming an identical response factor for GDGTs.

241

242 **3 Results and Discussion**

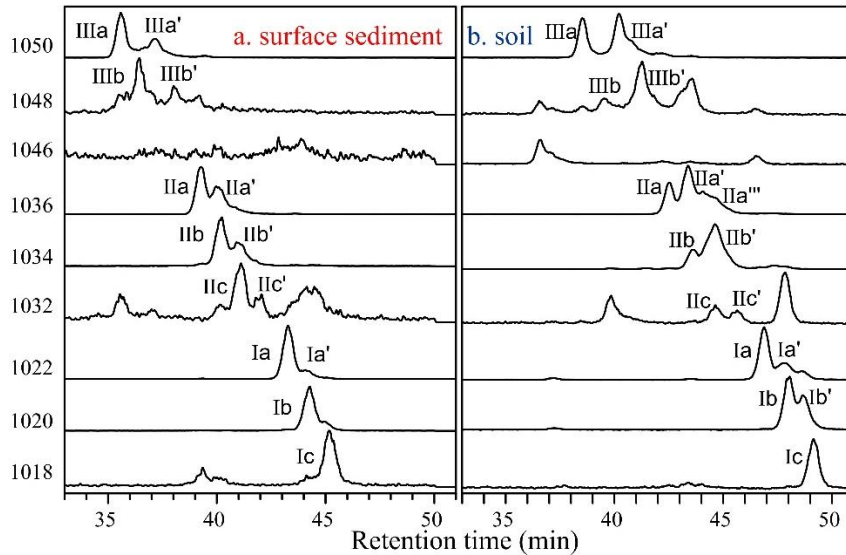
243 *3.1. Concentration and distribution of brGDGTs in the sediment core and catchment soils*

244 BrGDGTs were detected in both the catchment soils and the downcore sediments. The average
245 concentration of brGDGTs in the catchment soils (0.07 ng g⁻¹dw) was lower than in the surficial
246 core sediments (0.70 ng g⁻¹dw). In the soil samples, pentamethylated brGDGTs were generally
247 the most abundant (55.33%), followed by tetramethylated brGDGTs (23.60%) and
248 hexamethylated brGDGTs (21.07%) (Fig. S2). The relative amount of cyclopentane ring-
249 containing brGDGTs in the soil samples was generally low (24.34%) and it was sometimes too
250 low to be detected, especially the fractions of IIIb, IIIb', IIIc, IIIc', IIc and IIc'. In the downcore
251 sediments, the relative abundant of tetramethylated brGDGTs (43.84%) was like that of
252 pentamethylated brGDGTs (41.93%), and hexamethylated brGDGTs were the least abundant
253 (14.22%) (Fig. S2). The relative abundant of cyclopentane ring-containing brGDGTs in the
254 downcore sediments (67.82%) was lower than that in the catchment soils.

255 3.2 *In situ* production of brGDGTs in Gahai lake

256 Although lacustrine brGDGTs have great potential for quantitatively reconstructing terrestrial
257 paleotemperatures, uncertainties about their sources in lacustrine environments are a major
258 factor limiting their application (Tierney and Russell, 2009; Cao et al., 2020; Sun et al., 2011;
259 Sinninghe Damsté et al., 2009; Buckles et al., 2014). To investigate the origin and
260 characteristics of brGDGTs in the Gahai lake sediments, we examined the distributions and
261 concentrations of brGDGTs in the sediments and catchment soils and found notable differences
262 between them. First, as described in the previous section, the average content of brGDGTs in
263 the catchment soils was ~10% that of the surficial lake sediments, suggesting the absence of
264 large-scale allochthonous inputs from the catchment soils. Second, the brGDGTs distributions
265 in the downcore sediments were quite different from those in the catchment soils, which
266 suggests a substantial autochthonous brGDGTs contribution to the lake sediments (Fig. 3 and
267 Fig. S2). Moreover, the ratios of 6-methyl brGDGTs to 5-methyl GDGTs (IR_{6ME}) in the soils
268 and sediments, calculated according to the formula proposed by De Jonge et al. (2014), were
269 different. In the soil samples, IR_{6ME} varied between 0.54 and 0.57 and the average ratio in the
270 downcore samples was 0.26, varying between 0.18 and 0.47. Third, the in-situ production of
271 brGDGTs in Gahai lake is suggested by the discrepancies in the degree of methylation
272 (MBT'_{5ME}) between the soils and surface sediments. The average value of MBT'_{5ME} in the
273 Gahai lake surface sediments was 0.48, which is clearly higher than in the catchment soils,
274 with the range of 0.32–0.35. Fourth, and potentially the most significant, the IIIb' and Ib'
275 compounds are present in the catchments soil but not in the Gahai lake surficial sediments,
276 which may be direct evidence of an autochthonous brGDGTs contribution in the lacustrine

277 environment (Fig. 3), and a lower proportion of soil-derived brGDGTs input. Therefore, we
278 conclude that the brGDGTs in the Gahai lake sediments are mainly of in-situ origin.



279

280 **Fig. 3** Representative high-performance liquid chromatography/atmospheric pressure
281 chemical ionization-mass spectrometry (HPLC/APCIMS) chromatograms of brGDGTs
282 from (a) surface sediments from Gahai lake, and (b) soils in the catchment of Gahai
283 lake.

284

285 3.3 brGDGTs-temperature calibration and Holocene temperature reconstruction

286 Gahai is a shallow lake in the eastern Tibetan Plateau that is typically completely frozen during
287 winter and spring. Local meteorological data indicate that the average snowfall period lasts for
288 269 days, with around 50 days of continuous snowfall (Luqu County Local Chronicles
289 Compilation Committee, 2006). The freezing of the lake surface begins in late October each
290 year and gradually thaws starting from May of the following year. As a result, the light
291 transmittance and oxygen content in the lake water are reduced during the freezing season,
292 leading to decreased nutrient levels, which severely hinder the growth of autotrophic

293 microorganisms. Although the bacteria responsible for producing brGDGTs have not been
294 thoroughly characterized, the abundance of heterotrophic bacteria will likely decrease due to
295 the reduced autotrophic biomass during the winter and spring ice-covered period. The
296 weakened light penetration, decreased oxygen levels, and lack of nutrient replenishment during
297 the frozen period significantly impact the growth of autochthonous microorganisms.

298

299 Furthermore, some research suggests that the production of brGDGTs might be related to
300 factors such as water depth, seasonal alternation of water column mixing and stratification
301 (Loomis et al., 2014; Van Bree et al., 2020). During the summer and autumn seasons when the
302 lake ice melts and the water becomes more mobile, the nutrient content increases, resulting in
303 elevated lake biomass, moreover, the oxygen levels at the bottom of Gahai lake are not expected
304 to be too high, which could further contribute to the proliferation of brGDGT-producing
305 bacteria, potentially leading to an increase in the brGDGT-producing bacteria (Weber et al.,
306 2018). Therefore, brGDGTs in Gahai lake may provide records of the average temperature
307 during the ice-free months of the summer and autumn seasons.

308

309 Additionally, the presence of the frozen lake surface during winter creates a thermal barrier,
310 impeding the exchange of heat between the lake water and the atmosphere. Consequently, any
311 brGDGTs generated within the lake water during this period lose their ability to accurately
312 reflect atmospheric temperature variations (Sun et al., 2021; Zhang et al., 2022a). Thus, they
313 were no longer able to track atmospheric temperature changes during the frozen season. So, we
314 prefer to use Gahai brGDGTs to reconstruct temperatures during the summer and ice-free

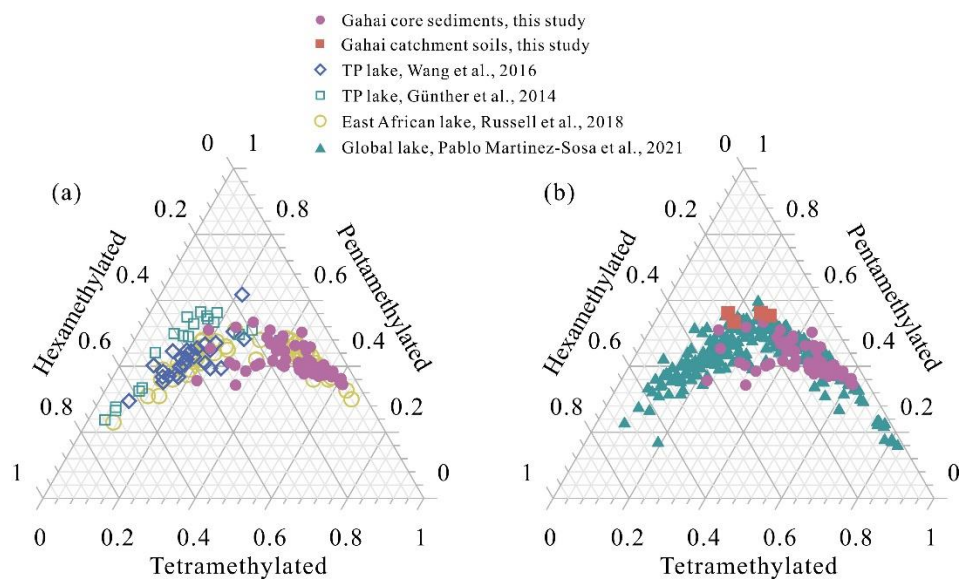
315 seasons. For this purpose, we employed the new Bayesian calibration for the mean temperature
316 of the Months Above Freezing (MAF), as proposed by Martínez-Sosa et al. (2021), to derive a
317 MAF for Gahai lake.

318
319 To assess the accuracy of this calibration approach, we compared the fractional abundances of
320 summed tetra-, penta-, and hexamethylated brGDGTs in Gahai lake sediments with other
321 datasets (Fig. 4). These datasets include lake sediments from the Tibetan Plateau (Günther et
322 al., 2014; Wang et al., 2016), East Africa (Russell et al., 2018), and global lakes (Martínez-
323 Sosa et al., 2021). The distribution pattern of Gahai core sediments is distinctly remarkable
324 compared to that of other lake sediments within the Tibetan Plateau, even though they share a
325 common regional origin (Fig. 4). However, its resemblance to the global distribution of
326 brGDGTs in lake sediments is evident. Notably, the calibration developed by Martínez-Sosa et
327 al. (2021) is based on brGDGTs from a global lake dataset.

328
329 Using calibration of Martínez-Sosa's et al. (2021), we reconstructed the surface sediment
330 temperature of Gahai lake, resulting in a temperature estimate of 9.4°C. This reconstructed
331 temperature closely matches the ice-free season temperature recorded by meteorological
332 stations in the Gahai region (8.8°C for May to September). Furthermore, considering the
333 significant contribution of autochthonous brGDGTs in Gahai lake, we also attempted to
334 reconstruct the Holocene paleotemperature record using previously published lake-specific
335 brGDGTs-temperature calibrations (e.g., Günther et al., 2014; Martínez-Sosa et al., 2021;
336 Russell et al., 2018; Sun et al., 2011; Wang et al., 2016). As depicted in Fig. S3, most of these

337 calibrations exhibit qualitatively similar temperature change patterns when applied to the
 338 sediment core from Gahai Lake. This similarity arises from their shared same principles, just
 339 utilizing distinct datasets, resulting in records that display analogous trends but vary in absolute
 340 temperatures.

341



342

343 **Fig. 4** Comparison of the fractional abundances of tetramethylated, pentamethylated, and
 344 hexamethylated bGDGTs in sediment core samples from Gahai with lake surface
 345 sediments from the Tibetan Plateau (Wang et al., 2016; Günther et al., 2014), East Africa
 346 (Russell et al., 2018), and worldwide (Martínez-Sosa et al., 2021).

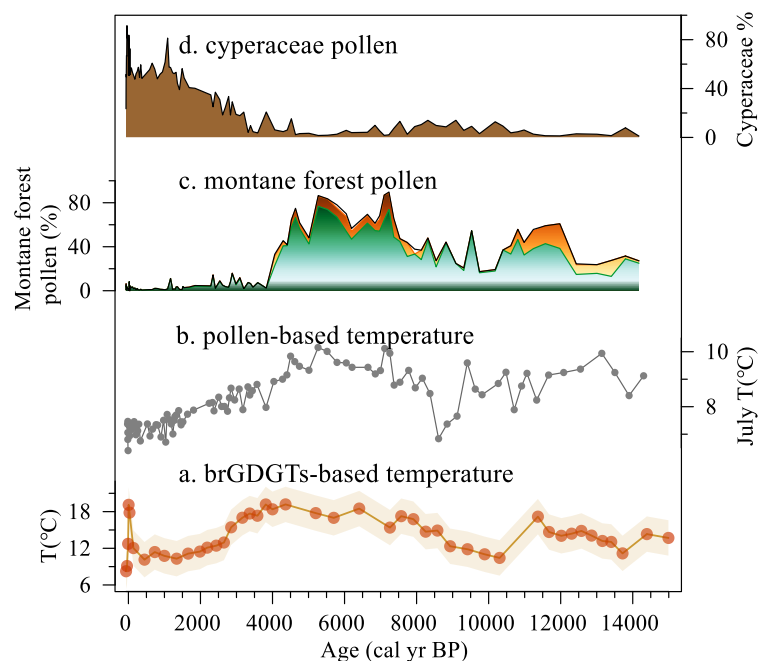
347

348 The depth interval of 191–279 cm in the Gahai sediment core represents an interval of rapid
 349 allocthonous sedimentation, or alternatively a slump, and therefore the results for the
 350 corresponding time interval of 20–15 ka may be unreliable. Thus, our temperature record of
 351 Months Above Freezing from the eastern TP spans the past 15 ka, with the average temperature
 352 of 4°C, as shown in Fig. 5a. Within the range of age uncertainties, weak warming occurred
 353 during 14.8–11.8 ka, likely to corresponding to the Bølling–Allerød (B/A) interstadial. A minor

354 cold reversal occurred during 11.8–10.5 ka, potentially corresponding to the Younger Dryas
355 (YD) event. Notably, the samples collected between 11.8 ka and 10.5 ka exhibited GDGT
356 concentrations below the detection limit. Therefore, we directly linked the temperature
357 reconstructions at the two aforementioned time points, ~11.8 ka and ~10.5 ka, resulting in the
358 lowest temperature of this time period appearing around 10.5 ka. This may cause a time lag
359 with the occurrence of the YD event. The temperature record indicates a colder period during
360 11.5–8.0 ka. During 8.0–3.5 ka, Gahai experienced a stable warm period with the average
361 temperature of ~16.5°C, after which the temperature decreased gradually. Overall, the
362 maximum temperature difference since 15 ka was ~10°C. As for the absolute temperature
363 changes since 15,000 yr, although some influential studies indicate a warming of
364 approximately 6.1–7°C from the deglaciation onset to preindustrial times (Tierney et al., 2020;
365 Osman et al., 2021). However, these results are based on global mean sea surface temperatures.
366 Our reconstructed temperature range is about 10°C, considering the remarkable ‘elevation-
367 dependent warming’ observed in high-altitude regions compared to low-altitude areas
368 (Mountain Initiative EDW Working Group, 2015). Thus, this range could be accurate.
369 Nevertheless, we do not rule out the possibility that our temperature reconstruction may exhibit
370 an overestimation. Aside from potential uncertainties associated with the biomarkers
371 themselves, calibrations may also considerably influence the observed amplitude. We
372 examined temperature variations reconstructed using different calibrations (Fig. S3), with the
373 smallest range being 6°C and the largest being 12°C. Undoubtedly, further efforts are needed
374 to constrain the inherent uncertainties related to biomarker-based temperature reconstructions.
375

376 3.4 Holocene temperature changes on the eastern edge of TP and their origin

377 Despite the difference in amplitude, the temperature record of Months Above Freezing from
378 Gahai resembles the pollen record and the pollen-based temperature reconstruction from the
379 same site (Fig. 5) (Wang et al., 2022). However, the brGDGTs-based Holocene Thermal
380 Maximum (HTM) lags the pollen-based reconstruction (Fig. 5a, b). Wang et al. (2022) used a
381 weighted-averaging partial least regression approach to produce a temperature record for Gahai,
382 based on a modern pollen dataset (n=731) from the eastern TP. Assessment of the statistical
383 significance of the pollen-based climate variables for Gahai suggests that the mean July
384 temperature is the most important environmental factor influencing the fossil pollen
385 assemblages. The brGDGTs in Gahai are indicative of summer and autumn temperatures, and
386 the mismatch between the temperature records inferred from brGDGTs and the pollen record
387 may be attributed to the difference between the solar irradiance during June–October and that
388 during July. A detailed analysis of this topic will be undertaken in the subsequent section.



389

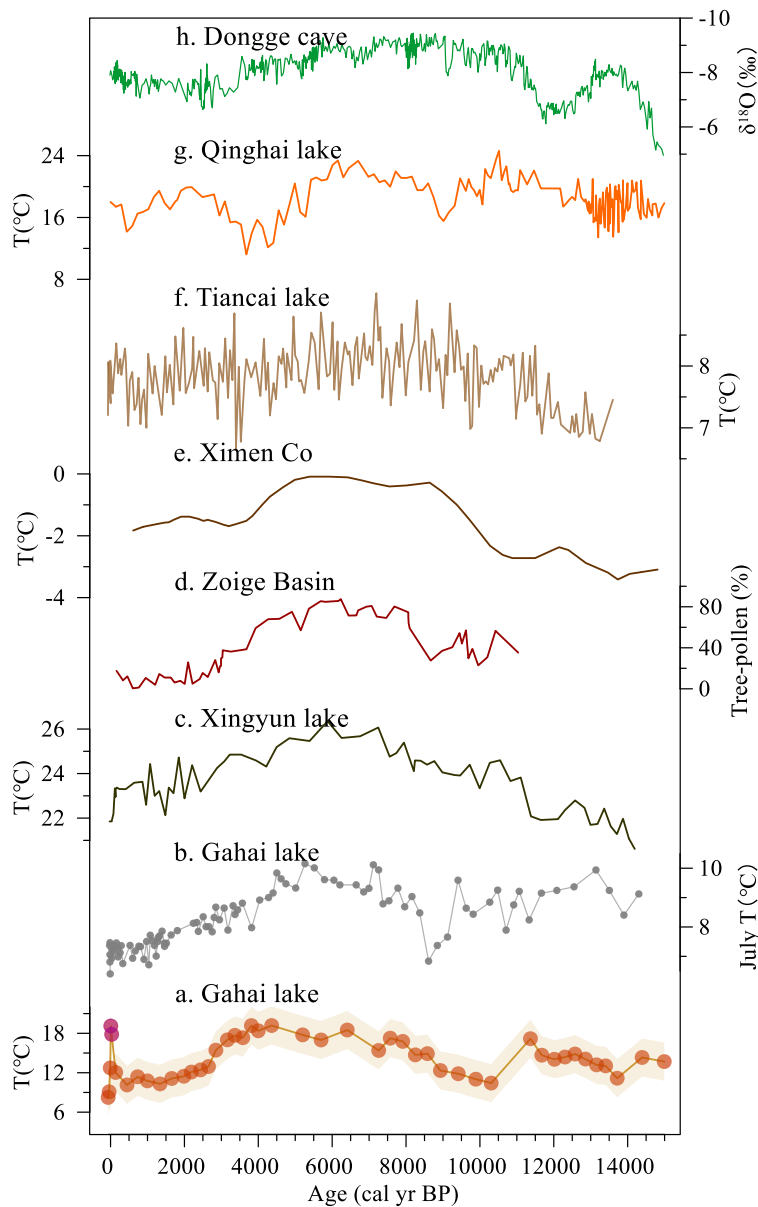
390 **Fig. 5** Comparison of multiproxy records from Gahai lake. (a) brGDGTs-based MAF (this

391 study). (b) Temperature of the warmest month (July) based on pollen assemblages
392 (Wang et al., 2022). (c, d) Pollen-reconstructed montane forest (*Pinus*, *Picea*, *Abies*) and
393 Cyperaceae pollen record (Wang et al., 2022).

394

395 The brGDGTs-based temperature record from Gahai confirms the occurrence of a climate
396 optimum in the mid-Holocene on the northeast Tibetan Plateau, which is consistent with several
397 other pollen and pollen-reconstructed temperature records from the fringe areas of the Asian
398 summer monsoon (Fig. 6), suggesting that it is a reliable representation of Holocene
399 temperature changes in this region. For example, pollen-based temperature reconstructions
400 from Xingyun lake and Ximen Co on the eastern TP show a early to middle HTM (9–4 ka) and
401 a cooling trend thereafter (Fig. 6c, e) (Wu et al., 2018; Herzschuh et al., 2014; Wang et al.,
402 2021a). Additionally, lake water temperature reconstructions based on subfossil chironomids
403 from Tiancai lake (Fig. 6f) (Zhang et al., 2017; Zhang et al., 2019a) and alkenones from
404 Qinghai lake (Fig. 6g) (Hou et al., 2016) show the same trends during the past 15 ka, as also
405 shown by other pollen-based temperature records from the TP (Chen et al., 2020). Pollen,
406 chironomids and alkenones mainly respond to the growing season temperatures in middle and
407 high latitudes, and thus the reconstructed temperature records are consistent with the variations
408 in summer solar irradiance. Similar variations were documented in temperature reconstructions
409 at a global scale (Marcott et al., 2013; Cartapanis et al., 2022). Nevertheless, the timing and
410 amplitude of the Gahai temperature fluctuations differ from those of other temperature records
411 from this region (Fig. 6). These discrepancies may be the result of the chronological
412 uncertainties of these records, and related to differences in the seasonal and spatial responses

413 to climate forcing and feedbacks.

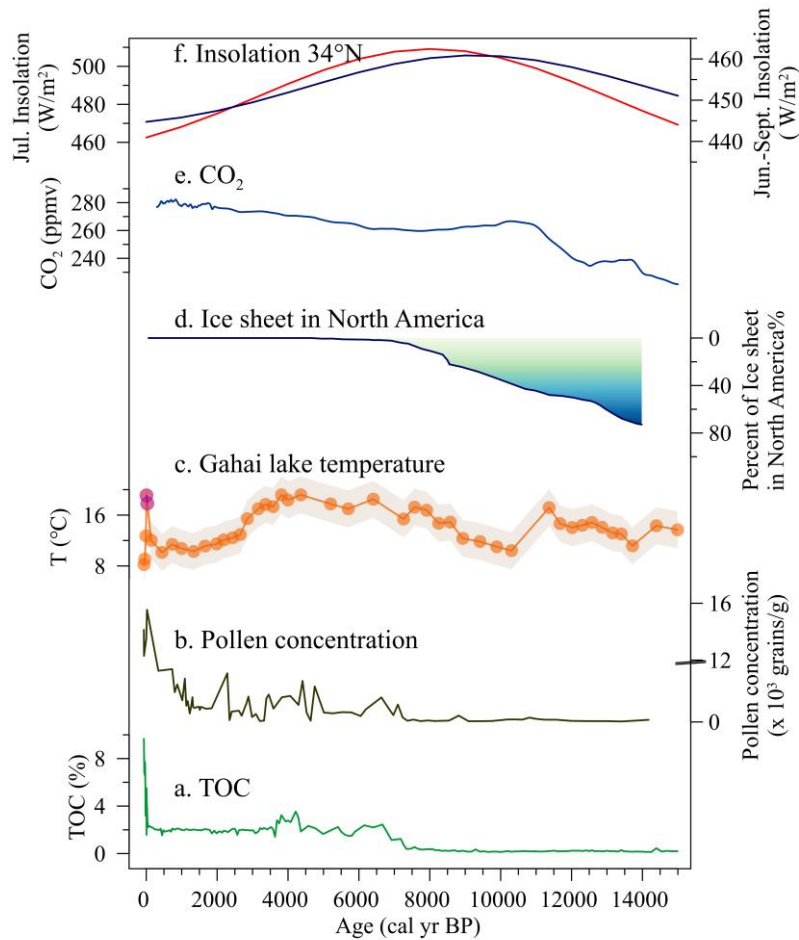


414

415 **Fig. 6** Comparison of temperature at Gahai and other records from the eastern edge of the
416 Tibetan Plateau. (a) brGDGTs-based MAF at Gahai, the purple dots may indicate
417 unreliable temperature changes influenced by human activities (this study). (b)
418 Temperature of the warmest month (July) based on pollen data from Gahai (Wang et al.,
419 2022). (c) Pollen-based temperature at Xingyun lake (Wu et al., 2018). (d) Tree pollen
420 percentages from the Hongyuan peatland in the southern Zoige Basin (Zhou et al.,
421 2010). (e) Pollen-based temperature at Ximen Co (Herzschuh et al., 2014). (f)
422 Chironomid-based temperature at Tiancai lake (Zhang et al., 2017, 2019a). (g)

423 Alkenone-based temperature at Qinghai lake (Hou et al., 2016). (h) Stalagmite $\delta^{18}\text{O}$
424 record of Donge cave (Dykoski et al., 2005).

425



426

427 **Fig. 7** Temperature fluctuations and forcing factors during the Holocene. (a, b) TOC content

428 and pollen concentrations from Gahai (Wang et al., 2022). (c) brGDGTs-based MAF

429 from Gahai, the purple dots may indicate unreliable temperature changes influenced by

430 human activities (this study). (d) Percentage of the remnant Laurentide ice sheet in

431 North America relative to the Last Glacial Maximum (Dyke, 2004). (e) Variation of

432 atmospheric CO₂ content (Monnin et al., 2004). (f) Mean insolation during July (W/m²)

433 (navy blue curve) and mean insolation during ice-free months (W/m²) at 34 °N (red

434 curve) (Berger and Loutre, 1991; Berger et al., 2010).

435

436 The temperature record in Gahai during the early Holocene fails to closely track the Northern
437 Hemisphere insolation trend, and there is also a time lag. The pollen-based temperature record
438 for Xingyun Lake in southwestern China also shows lower temperatures in the early Holocene
439 (Fig. 6c). The albedo effect caused by the increased cloud cover may be the reason for the early
440 Holocene decrease in summer temperatures (Wu et al., 2018). However, the pollen record from
441 Gahai indicates dry conditions during the early Holocene (Wang et al., 2022), and cloud cover
442 may not be the primary factor responsible for the low temperatures at this time. The melting of
443 Northern Hemisphere ice sheets during the early Holocene would weaken the Atlantic
444 Meridional Overturning Circulation (AMOC) and potentially also the global thermohaline
445 circulation. This would lead to a reduction in the amount of heat transport by the North Atlantic
446 warm current to high-latitude regions and a cooling in middle to high latitudes of the Northern
447 Hemisphere.. The persistence of the Laurentide ice sheet into the early Holocene maintained
448 the regional albedo, as well as discharging meltwater into the North Atlantic (Fig. 7d) (Dyke,
449 2004). Furthermore, the cooling during the early Holocene followed by the warming trend in
450 the mid-Holocene potentially correlates with significant fluctuations in CO₂ concentrations
451 within these intervals (Fig. 7e) (Monnin et al., 2004). In addition, a Holocene temperature
452 simulation showed that global warming was more pronounced when dust factors were excluded
453 from the simulation (Liu et al. (2018). The record of insoluble particles in the Greenland GISP2
454 ice core indicates relatively high concentrations of atmospheric aerosols in the early Holocene
455 (Zielinski and Mershon, 1997), which would have weakened summer solar irradiation via

456 radiative feedback, leading to the cool temperatures during this period. In essence, temperature,
457 especially seasonal variations like the Gahai ice-free temperature in the eastern TP, is
458 influenced by multifaceted factors including astronomical forcing, CO₂, and ice sheets.
459 Temperature exhibits varied sensitivities in response to these factors, while both insolation and
460 CO₂ exert considerable and favorable impacts on summer temperature patterns (Lyu and Yin,
461 2022). These factors may together have caused the early Holocene temperature decline at Gahai
462 Lake, which slightly delayed the onset of the Holocene Warm Period.

463

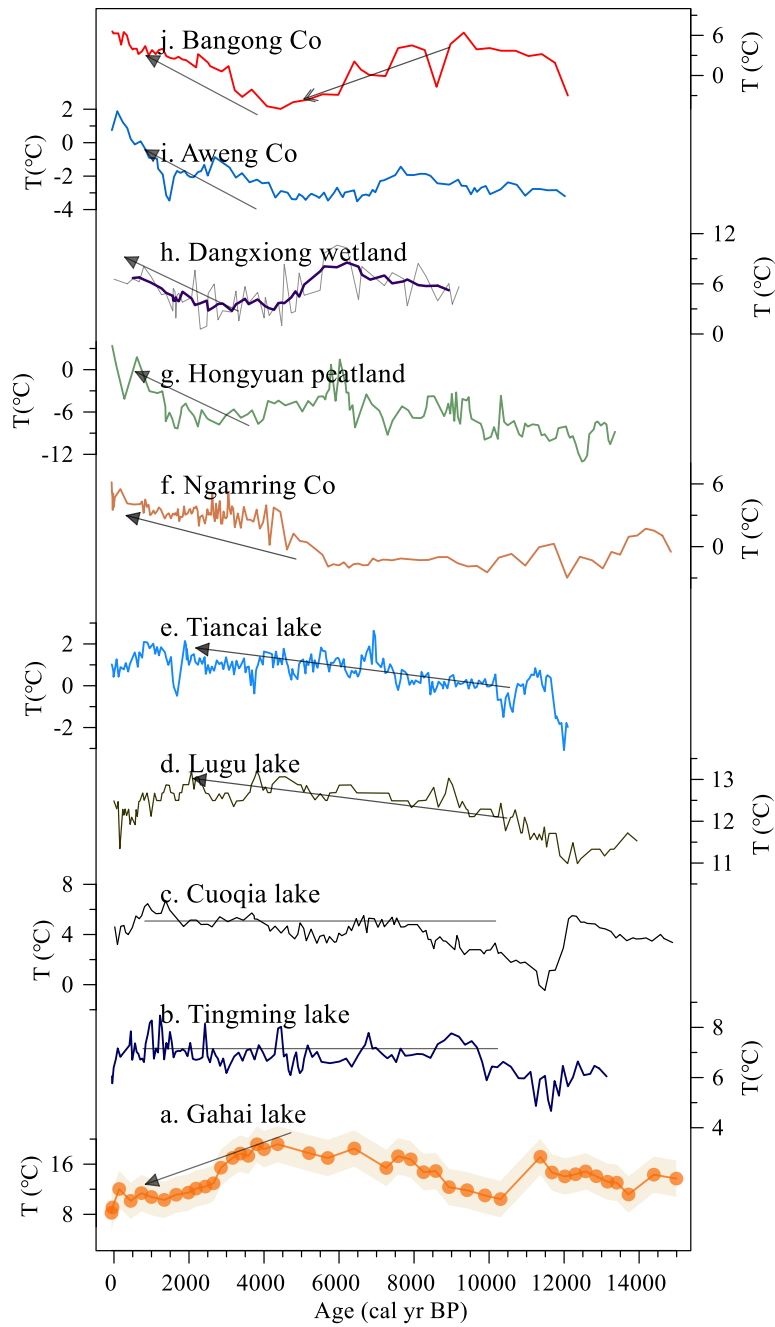
464 A notable and rapid temperature increase is evident at Gahai in recent decades, which differs
465 from the other records (Fig. 7c). Moreover, there are notable increases in pollen concentration,
466 TOC, and TN (Fig. 7a, b) in the Gahai sediment core, indicating intensive local human activities
467 like grazing and tourism, which may be the primary cause of the environmental changes in this
468 region (Wang et al., 2022). This intensive human activity may have reduced the ability of the
469 brGDGTs to record the natural temperature background. These observations emphasize the
470 important impact of human activities on climate proxies and the need to carefully consider their
471 effect on temperature reconstructions.

472

473 *3.5 Spatiotemporal pattern of brGDGTs-based TP temperatures*

474 In addition to comparing the Gahai temperature with the summer temperature records from the
475 eastern TP and its surrounding areas, we compiled and reviewed published Holocene
476 brGDGTs-based quantitative temperature records from across the TP. As shown in Fig. 8, with
477 the increasing number of these records for the TP, the differences between the results have

478 become more pronounced. The brGDGTs records from lakes in the central and western parts
479 of the plateau show higher temperatures in the early and late Holocene, and lower temperatures
480 in the middle Holocene (Wang et al., 2021c; Li et al., 2017; He et al., 2020), while the brGDGTs
481 records from lakes in the southern and south-eastern parts of the TP show a warming trend
482 throughout the Holocene (Sun et al., 2022; Feng et al., 2022). In addition, brGDGTs in Cuoqia
483 lake and Tingming lake, on the south-eastern TP, recorded the ice-free season temperature,
484 which was relatively stable during the Holocene (Sun et al., 2021; Zhang et al., 2022a).
485 However, our temperature record from Gahai is different from the above records and resembles
486 summer temperature changes during the Holocene (Chen et al., 2020). This is because the
487 brGDGTs record from Lake Gahai represents warm season temperatures, which adds to its
488 reliability.



489

490 **Fig. 8** Comparison of Holocene temperature based on brGDGTs at Gahai (a) and other

491 records from around the TP. Reconstructed ice-free-season temperatures from (b)

492 Tingming lake (Sun et al., 2021), (c) Cuoqia lake (Zhang et al., 2022a). Reconstructed

493 annual temperature from (d) Lugu lake (Zhao et al., 2021b), (e) Tiancai lake (Feng et al.,

494 2022), (f) Ngamring Co(Sun et al., 2022), (g) Hongyuan peatland (Yan et al., 2021). (h)

495 Dangxiong wetland (Cheung et al., 2017), (i) Aweng Co (Li et al., 2017), (j) Bangong

496 Co (Wang et al., 2021c).

497

498 We suggest that the complexity of Holocene temperature patterns recorded by brGDGTs in TP
499 lakes is primarily due to the ambiguity of brGDGTs in these lakes, as well as to the spatial
500 heterogeneity of climate change across the TP. This ambiguity can be attributed to several
501 factors. First, the origin of brGDGTs in lakes remains an uncertain factor in temperature
502 reconstruction. An increasing number of studies indicate the occurrence of a remarkable
503 amount of autochthonous brGDGTs in lakes, but their abundance in soil can also affect the
504 distribution of brGDGTs in lakes due to their supply via soil erosion (e.g., Tierney and Russell,
505 2009; Weber et al., 2015; Wang et al., 2023). In fact, even within the same lake (e.g.,
506 Tengchongqinghai lake in southwestern China), two studies reached inconsistent conclusions
507 regarding the origin of brGDGTs (Tian et al., 2019; Zhao et al., 2021b), possibly because the
508 niches of certain brGDGTs may expand or contract compared to other locations within a lake.
509 Therefore, it is important to conduct detailed modern process studies to accurately assess the
510 sources of brGDGTs in lakes, especially with regard to evaluating the proportion of
511 autochthonous brGDGTs (Wang et al., 2023; Martin et al., 2020). Second, brGDGTs may show
512 a seasonal signal. Current brGDGTs–temperature calibrations for lakes reflect the annual
513 average temperature (Sun et al., 2011; De Jonge et al., 2014), as well as the growing season
514 temperature (Sun et al., 2011; Dang et al., 2018) and the ice-free season temperature (Martínez-
515 Sosa et al., 2021; Zhang et al., 2022a). Thus, there is no consensus regarding whether the
516 brGDGTs have a seasonal bias, and it is necessary to conduct continuous, high-resolution
517 seasonal investigations of lakes on the Tibetan Plateau to comprehensively elucidate the

518 seasonal characteristics of brGDGTs. This can enhance the accuracy of regional temperature
519 reconstruction and may help reconcile the complex temperature patterns observed on the
520 Tibetan Plateau. Third, the factors affecting the distribution of brGDGTs in lakes are complex,
521 including not only temperature, pH and salinity but also oxygen content, water depth, and so
522 on (Wang et al., 2021b; Wang et al., 2016). The distribution of brGDGTs in lakes is significantly
523 influenced by the hydrological and physical properties of the lakes, and thus it is necessary to
524 attain a more comprehensive understanding of the characteristics of the lakes in the study area
525 and their effects on brGDGTs. Fourth, different brGDGTs–temperature calibrations may lead
526 to markable differences in both the amplitude and trend of temperature from the same dataset
527 (Wang et al., 2016; Feng et al., 2019). One reason for this is the deviation between in-situ
528 measured temperature and atmospheric temperature (Wang et al., 2020). Thus, selecting an
529 appropriate calibration and attempting to establish a brGDGTs-in situ temperature calibration
530 are effective means of enhancing the reliability of brGDGTs-based temperature reconstructions.

531

532 **4 Conclusions**

533 We present a quantitative, brGDGTs-based seasonal paleotemperature record over the last 15
534 ka from the sediments of a shallow lake on the eastern Tibetan Plateau. Our reconstruction
535 resembles the summer temperature trend, with the Holocene Thermal Maximum occurring
536 during 8–3.5 ka. There is a lag between our brGDGTs-based reconstruction and pollen-based
537 temperature recorded in the same sediment core, indicating a seasonal bias between different
538 proxies. Since 3.5 ka, the temperature decreased gradually, and the surficial sediments reliably
539 recorded the warm season temperature during the current period in the Gahai Lake region.

540 However, intensive local human activity during the last century has affected the distribution of
541 brGDGTs, resulting in temperature deviations recorded by brGDGTs. However, the
542 implementation of environmental protection policies have reduced this anthropogenic signal.
543 Our findings help better understand the seasonal signal of brGDGTs in shallow lakes and
544 provide important data for improving projections of terrestrial climate change at high
545 elevations.

546

547 We also investigated previously published brGDGTs-based Holocene temperature records on
548 the TP to determine the pattern of brGDGTs-based temperature changes and the possible causes
549 of the differences between reconstructions. We emphasize the need for the careful examination
550 of both the source and behavior of these compounds in lacustrine environments and lake status,
551 prior to the application of brGDGTs proxies in paleolimnological reconstruction.

552

553 **Data availability**

554 The data used in this study can be obtained from the corresponding author Juzhi Hou
555 (houjz@itpcas.ac.cn).

556

557 **Author contributions**

558 Xiaohuan Hou did the experiments, analyzed the data and wrote the manuscript. Nannan Wang,
559 Zhe Sun, Kan Yuan and Xianyong Cao participated in sample collecting and data analysis.
560 Juzhi Hou designed this study and led the interpretation. All authors commented on and
561 improved the manuscript.

562

563 **Competing interests**

564 The contact author has declared that none of the authors has any competing interests.

565

566 **Acknowledgements**

567 This work was financially supported by the National Natural Science Foundation of China

568 (42025103, 41877459) and the Second Tibetan Plateau Scientific Expedition and Research

569 (2019QZKK0601). We would like to thank Jan Bloemendal for the help with language

570 editing.

571

572 **References**

573

574 Berger, A. and Loutre, M. F.: Insolation values for the climate of the last 10000000 years, *Quaternary Science*
575 *Reviews*, 10, 297-317, 10.1016/0277-3791(91)90033-q, 1991.

576 Berger, A., Loutre, M. F., and Yin, Q. Z.: Total irradiation during any time interval of the year using elliptic
577 integrals, *Quaternary Science Reviews*, 29, 1968-1982, 10.1016/j.quascirev.2010.05.007, 2010.

578 Bova, S., Rosenthal, Y., Liu, Z., Godad, S. P., and Yan, M.: Seasonal origin of the thermal maxima at the Holocene
579 and the last interglacial, *Nature*, 589, 548-553, 10.1038/s41586-020-03155-x, 2021.

580 Buckles, L. K., Weijers, J. W. H., Verschuren, D., and Damste, J. S. S.: Sources of core and intact branched
581 tetraether membrane lipids in the lacustrine environment: Anatomy of Lake Challa and its catchment, equatorial
582 East Africa, *Geochimica Et Cosmochimica Acta*, 140, 106-126, 10.1016/j.gca.2014.04.042, 2014.

583 Cao, J., Rao, Z., Shi, F., and Jia, G.: Ice formation on lake surfaces in winter causes warm-season bias of lacustrine
584 brGDGT temperature estimates, *Biogeosciences*, 17, 2521-2536, 10.5194/bg-17-2521-2020, 2020.

585 Cartapanis, O., Jonkers, L., Moffa-Sanchez, P., Jaccard, S. L., and de Vernal, A.: Complex spatio-temporal
586 structure of the Holocene Thermal Maximum, *Nat Commun*, 13, 5662, 10.1038/s41467-022-33362-1, 2022.

587 Chen, D., Xu, B., Yao, T., Guo, Z., Cui, P., Chen, F., Zhang, R., Zhang, X., Zhang, Y., Fan, J., Hou, Z., and Zhang,
588 T.: Assessment of past, present and future environmental changes on the Tibetan Plateau, *Chinese Science Bulletin*,
589 60, 3025-3035, 2015.

590 Chen, F., Yu, Z., Yang, M., Ito, E., Wang, S., Madsen, D. B., Huang, X., Zhao, Y., Sato, T., Birks, H. J. B., Boomer,
591 I., Chen, J., An, C., and Wünnemann, B.: Holocene moisture evolution in arid central Asia and its out-of-phase
592 relationship with Asian monsoon history, *Quaternary Science Reviews*, 27, 351-364,
593 10.1016/j.quascirev.2007.10.017, 2008.

594 Chen, F., Zhang, J., Liu, J., Cao, X., Hou, J., Zhu, L., Xu, X., Liu, X., Wang, M., Wu, D., Huang, L., Zeng, T.,
595 Zhang, S., Huang, W., Zhang, X., and Yang, K.: Climate change, vegetation history, and landscape responses on
596 the Tibetan Plateau during the Holocene: A comprehensive review, *Quaternary Science Reviews*, 243,
597 10.1016/j.quascirev.2020.106444, 2020.

598 Chen, Y., Zheng, F., Yang, H., Yang, W., Wu, R., Liu, X., Liang, H., Chen, H., Pei, H., Zhang, C., Pancost, R. D.,
599 and Zeng, Z.: The production of diverse brGDGTs by an Acidobacterium providing a physiological basis for
600 paleoclimate proxies, *Geochimica et Cosmochimica Acta*, 337, 155-165, 10.1016/j.gca.2022.08.033, 2022.

601 Cheung, M.-C., Zong, Y., Zheng, Z., Liu, Z., and Aitchison, J. C.: Holocene temperature and precipitation
602 variability on the central Tibetan Plateau revealed by multiple palaeo-climatic proxy records from an alpine
603 wetland sequence, *The Holocene*, 27, 1669-1681, 10.1177/0959683617702225, 2017.

604 Committee, L. C. L. C. C.: *Luqu County Chronicles*, Gansu Cultural Publishing House, Lanzhou, 71 pp.2006.

605 Crampton-Flood, E. D., Tierney, J. E., Peterse, F., Kirkels, F. M. S. A., and Damste, J. S. S.: BayMBT: A Bayesian
606 calibration model for branched glycerol dialkyl glycerol tetraethers in soils and peats, *Geochimica Et*
607 *Cosmochimica Acta*, 268, 142-159, 10.1016/j.gca.2019.09.043, 2020.

608 Dang, X., Ding, W., Yang, H., Pancost, R. D., Naafs, B. D. A., Xue, J., Lin, X., Lu, J., and Xie, S.: Different
609 temperature dependence of the bacterial brGDGT isomers in 35 Chinese lake sediments compared to that in soils,
610 *Organic Geochemistry*, 119, 72-79, 10.1016/j.orggeochem.2018.02.008, 2018.

611 De Jonge, C., Hopmans, E. C., Zell, C. I., Kim, J.-H., Schouten, S., and Sinninghe Damsté, J. S.: Occurrence and
612 abundance of 6-methyl branched glycerol dialkyl glycerol tetraethers in soils: Implications for palaeoclimate
613 reconstruction, *Geochimica et Cosmochimica Acta*, 141, 97-112, 10.1016/j.gca.2014.06.013, 2014.

614 Ding, S., Xu, Y., Wang, Y., He, Y., Hou, J., Chen, L., and He, J. S.: Distribution of branched glycerol dialkyl
615 glycerol tetraethers in surface soils of the Qinghai-Tibetan Plateau: implications of brGDGTs-based proxies in

616 cold and dry regions, *Biogeosciences*, 12, 3141-3151, 10.5194/bg-12-3141-2015, 2015.

617 Dong, Y., Wu, N., Li, F., Zhang, D., Zhang, Y., Shen, C., and Lu, H.: The Holocene temperature conundrum
618 answered by mollusk records from East Asia, *Nat Commun*, 13, 5153, 10.1038/s41467-022-32506-7, 2022.

619 Dyke, A. S.: An outline of North American deglaciation with emphasis on central and northern Canada,
620 Quaternary Glaciations-Extent and Chronology, Pt 2: North America, 2, 373-424, 10.1016/s1571-0866(04)80209-
621 4, 2004.

622 Dykoski, C. A., Edwards, R. L., Cheng, H., Yuan, D. X., Cai, Y. J., Zhang, M. L., Lin, Y. S., Qing, J. M., An, Z.
623 S., and Revenaugh, J.: A high-resolution, absolute-dated Holocene and deglacial Asian monsoon record from
624 Dongge Cave, China, *Earth and Planetary Science Letters*, 233, 71-86, 10.1016/j.epsl.2005.01.036, 2005.

625 Feng, X., Zhao, C., D'Andrea, W. J., Liang, J., Zhou, A., and Shen, J.: Temperature fluctuations during the
626 Common Era in subtropical southwestern China inferred from brGDGTs in a remote alpine lake, *Earth and
627 Planetary Science Letters*, 510, 26-36, 10.1016/j.epsl.2018.12.028, 2019.

628 Feng, X., Zhao, C., D'Andrea, W. J., Hou, J., Yang, X., Xiao, X., Shen, J., Duan, Y., and Chen, F.: Evidence for a
629 Relatively Warm Mid-to Late Holocene on the Southeastern Tibetan Plateau, *Geophysical Research Letters*, 49,
630 10.1029/2022gl098740, 2022.

631 Group, M. I. E. W.: Elevation-dependent warming in mountain regions of the world, *Nature Climate Change*, 5,
632 424-430, 10.1038/nclimate2563, 2015.

633 Günther, F., Thiele, A., Gleixner, G., Xu, B., Yao, T., and Schouten, S.: Distribution of bacterial and archaeal ether
634 lipids in soils and surface sediments of Tibetan lakes: Implications for GDGT-based proxies in saline high
635 mountain lakes, *Organic Geochemistry*, 67, 19-30, 10.1016/j.orggeochem.2013.11.014, 2014.

636 Halamka, T. A., Raberg, J. H., McFarlin, J. M., Younkin, A. D., Mulligan, C., Liu, X. L., and Kopf, S. H.:
637 Production of diverse brGDGTs by *Acidobacterium Solibacter usitatus* in response to temperature, pH, and O₂
638 provides a culturing perspective on brGDGT proxies and biosynthesis, *Geobiology*, 10.1111/gbi.12525, 2022.

639 He, Y., Hou, J., Wang, M., Li, X., Liang, J., Xie, S., and Jin, Y.: Temperature Variation on the Central Tibetan
640 Plateau Revealed by Glycerol Dialkyl Glycerol Tetraethers From the Sediment Record of Lake Linggo Co Since
641 the Last Deglaciation, *Frontiers in Earth Science*, 8, 10.3389/feart.2020.574206, 2020.

642 Herzsuh, U., Borkowski, J., Schewe, J., Mischke, S., and Tian, F.: Moisture-advection feedback supports strong
643 early-to-mid Holocene monsoon climate on the eastern Tibetan Plateau as inferred from a pollen-based
644 reconstruction, *Palaeogeography, Palaeoclimatology, Palaeoecology*, 402, 44-54, 10.1016/j.palaeo.2014.02.022,
645 2014.

646 Hou, J., Li, C., and Lee, S.: The temperature record of the Holocene: progress and controversies, *Science Bulletin*,
647 10.1016/j.scib.2019.02.012, 2019.

648 Hou, J., Huang, Y., Zhao, J., Liu, Z., Colman, S., and An, Z.: Large Holocene summer temperature oscillations
649 and impact on the peopling of the northeastern Tibetan Plateau, *Geophysical Research Letters*, 43, 1323-1330,
650 10.1002/2015gl067317, 2016.

651 Huguet, C., Hopmans, E. C., Febo-Ayala, W., Thompson, D. H., Sinninghe Damsté, J. S., and Schouten, S.: An
652 improved method to determine the absolute abundance of glycerol dibiphytanyl glycerol tetraether lipids, *Organic
653 Geochemistry*, 37, 1036-1041, 10.1016/j.orggeochem.2006.05.008, 2006.

654 Kuang, X. and Jiao, J. J.: Review on climate change on the Tibetan Plateau during the last half century, *Journal of
655 Geophysical Research: Atmospheres*, 121, 3979-4007, 10.1002/2015jd024728, 2016.

656 Li, X., Wang, M., Zhang, Y., Lei, L., and Hou, J.: Holocene climatic and environmental change on the western
657 Tibetan Plateau revealed by glycerol dialkyl glycerol tetraethers and leaf wax deuterium-to-hydrogen ratios at
658 Aweng Co, *Quaternary Research*, 87, 455-467, 10.1017/qua.2017.9, 2017.

659 Liu, Y., Zhang, M., Liu, Z., Xia, Y., Huang, Y., Peng, Y., and Zhu, J.: A Possible Role of Dust in Resolving the

660 Holocene Temperature Conundrum, *Scientific Reports*, 8, 10.1038/s41598-018-22841-5, 2018.

661 Liu, Z. Y., Zhu, J., Rosenthal, Y., Zhang, X., Otto-Bliesner, B. L., Timmermann, A., Smith, R. S., Lohmann, G.,
662 Zheng, W. P., and Timm, O. E.: The Holocene temperature conundrum, *Proc. Natl. Acad. Sci. U. S. A.*, 111, E3501-
663 E3505, 10.1073/pnas.1407229111, 2014.

664 Loomis, S. E., Russell, J. M., Heuroux, A. M., D'Andrea, W. J., and Sinninghe Damsté, J. S.: Seasonal variability
665 of branched glycerol dialkyl glycerol tetraethers (brGDGTs) in a temperate lake system, *Geochimica et*
666 *Cosmochimica Acta*, 144, 173-187, 10.1016/j.gca.2014.08.027, 2014.

667 Lu, H., Wu, N., Liu, K.-b., Zhu, L., Yang, X., Yao, T., Wang, L., Li, Q., Liu, X., Shen, C., Li, X., Tong, G., and
668 Jiang, H.: Modern pollen distributions in Qinghai-Tibetan Plateau and the development of transfer functions for
669 reconstructing Holocene environmental changes, *Quaternary Science Reviews*, 30, 947-966,
670 10.1016/j.quascirev.2011.01.008, 2011.

671 Lyu, A. and Yin, Q. Z.: The spatial-temporal patterns of East Asian climate in response to insolation, CO₂ and ice
672 sheets during MIS-5, *Quaternary Science Reviews*, 293, 10.1016/j.quascirev.2022.107689, 2022.

673 Ma, W., Li, G., Song, J., Yan, L., and Wu, L.: Effect of Vegetation Degradation on Soil Organic Carbon Pool and
674 Carbon Pool Management Index in the Gahai Wetland, China, *Acta Agrestia Sinica*, 27, 687-694, 2019.

675 Marcott, S. A., Shakun, J. D., Clark, P. U., and Mix, A. C.: A Reconstruction of Regional and Global Temperature
676 for the Past 11,300 Years, *Science*, 339, 1198-1201, 10.1126/science.1228026, 2013.

677 Marsicek, J., Shuman, B. N., Bartlein, P. J., Shafer, S. L., and Brewer, S.: Reconciling divergent trends and
678 millennial variations in Holocene temperatures, *Nature*, 554, 92-+, 10.1038/nature25464, 2018.

679 Martin, C., Ménot, G., Thouveny, N., Peyron, O., Andrieu-Ponel, V., Montade, V., Davtian, N., Reille, M., and
680 Bard, E.: Early Holocene Thermal Maximum recorded by branched tetraethers and pollen in Western Europe
681 (Massif Central, France), *Quaternary Science Reviews*, 228, 106109, 10.1016/j.quascirev.2019.106109, 2020.

682 Martínez-Sosa, P., Tierney, J. E., Stefanescu, I. C., Dearing Crampton-Flood, E., Shuman, B. N., and Routsos, C.:
683 A global Bayesian temperature calibration for lacustrine brGDGTs, *Geochimica et Cosmochimica Acta*, 305, 87-
684 105, 10.1016/j.gca.2021.04.038, 2021.

685 Monnin, E., Steig, E. J., Siegenthaler, U., Kawamura, K., Schwander, J., Stauffer, B., Stocker, T. F., Morse, D. L.,
686 Barnola, J. M., Bellier, B., Raynaud, D., and Fischer, H.: Evidence for substantial accumulation rate variability in
687 Antarctica during the Holocene, through synchronization of CO₂ in the Taylor Dome, Dome C and DML ice cores,
688 *Earth and Planetary Science Letters*, 224, 45-54, 10.1016/j.epsl.2004.05.007, 2004.

689 Moser, K. A., Baron, J. S., Brahney, J., Oleksy, I. A., Saros, J. E., Hundey, E. J., Sadro, S., Kopáček, J., Sommaruga,
690 R., Kainz, M. J., Strecker, A. L., Chandra, S., Walters, D. M., Preston, D. L., Michelutti, N., Lepori, F., Spaulding,
691 S. A., Christianson, K. R., Melack, J. M., and Smol, J. P.: Mountain lakes: Eyes on global environmental change,
692 *Global and Planetary Change*, 178, 77-95, 10.1016/j.gloplacha.2019.04.001, 2019.

693 Opitz, S., Zhang, C., Herzsich, U., and Mischke, S.: Climate variability on the south-eastern Tibetan Plateau
694 since the Lateglacial based on a multiproxy approach from Lake Naleng – comparing pollen and non-pollen
695 signals, *Quaternary Science Reviews*, 115, 112-122, 10.1016/j.quascirev.2015.03.011, 2015.

696 Osman, M. B., Tierney, J. E., Zhu, J., Tardif, R., Hakim, G. J., King, J., and Poulsen, C. J.: Globally resolved
697 surface temperatures since the Last Glacial Maximum, *Nature*, 599, 239-244, 10.1038/s41586-021-03984-4, 2021.

698 Pang, H., Hou, S., Zhang, W., Wu, S., Jenk, T. M., Schwikowski, M., and Jouzel, J.: Temperature Trends in the
699 Northwestern Tibetan Plateau Constrained by Ice Core Water Isotopes Over the Past 7,000 Years, *Journal of*
700 *Geophysical Research-Atmospheres*, 125, 10.1029/2020jd032560, 2020.

701 Qiu, J.: The third pole, *Nature*, 454, 393-396, 10.1038/454393a, 2008.

702 Russell, J. M., Hopmans, E. C., Loomis, S. E., Liang, J., and Sinninghe Damsté, J. S.: Distributions of 5- and 6-
703 methyl branched glycerol dialkyl glycerol tetraethers (brGDGTs) in East African lake sediment: Effects of

704 temperature, pH, and new lacustrine paleotemperature calibrations, *Organic Geochemistry*, 117, 56-69,
705 10.1016/j.orggeochem.2017.12.003, 2018.

706 Sinninghe Damsté, J. S., Hopmans, E. C., Pancost, R. D., Schouten, S., and Geenevasen, J. A. J.: Newly discovered
707 non-isoprenoid glycerol dialkyl glycerol tetraether lipids in sediments, *Chemical Communications*, 1683-1684,
708 10.1039/b004517i, 2000.

709 Sinninghe Damsté, J. S., Ossebaar, J., Abbas, B., Schouten, S., and Verschuren, D.: Fluxes and distribution of
710 tetraether lipids in an equatorial African lake: Constraints on the application of the TEX86 palaeothermometer
711 and BIT index in lacustrine settings, *Geochimica et Cosmochimica Acta*, 73, 4232-4249,
712 10.1016/j.gca.2009.04.022, 2009.

713 Sun, Q., Chu, G., Liu, M., Xie, M., Li, S., Ling, Y., Wang, X., Shi, L., Jia, G., and Lü, H.: Distributions and
714 temperature dependence of branched glycerol dialkyl glycerol tetraethers in recent lacustrine sediments from
715 China and Nepal, *Journal of Geophysical Research*, 116, 10.1029/2010jg001365, 2011.

716 Sun, X., Zhao, C., Zhang, C., Feng, X., Yan, T., Yang, X., and Shen, J.: Seasonality in Holocene Temperature
717 Reconstructions in Southwestern China, *Paleoceanography and Paleoclimatology*, 36, 10.1029/2020pa004025,
718 2021.

719 Sun, Z., Hou, X., Ji, K., Yuan, K., Li, C., Wang, M., and Hou, J.: Potential winter-season bias of annual temperature
720 variations in monsoonal Tibetan Plateau since the last deglaciation, *Quaternary Science Reviews*, 292,
721 10.1016/j.quascirev.2022.107690, 2022.

722 Thompson, L. G., Yao, T., Davis, M. E., Henderson, K. A., MosleyThompson, E., Lin, P. N., Beer, J., Synal, H.
723 A., ColeDai, J., and Bolzan, J. F.: Tropical climate instability: The last glacial cycle from a Qinghai-Tibetan ice
724 core, *Science*, 276, 1821-1825, 10.1126/science.276.5320.1821, 1997.

725 Tian, L., Wang, M., Zhang, X., Yang, X., Zong, Y., Jia, G., Zheng, Z., and Man, M.: Synchronous change of
726 temperature and moisture over the past 50 ka in subtropical southwest China as indicated by biomarker records in
727 a crater lake, *Quaternary Science Reviews*, 212, 121-134, 10.1016/j.quascirev.2019.04.003, 2019.

728 Tierney, J. E. and Russell, J. M.: Distributions of branched GDGTs in a tropical lake system: Implications for
729 lacustrine application of the MBT/CBT paleoproxy, *Organic Geochemistry*, 40, 1032-1036,
730 10.1016/j.orggeochem.2009.04.014, 2009.

731 Tierney, J. E., Russell, J. M., Eggermont, H., Hopmans, E. C., Verschuren, D., and Sinninghe Damsté, J. S.:
732 Environmental controls on branched tetraether lipid distributions in tropical East African lake sediments,
733 *Geochimica et Cosmochimica Acta*, 74, 4902-4918, 10.1016/j.gca.2010.06.002, 2010.

734 Tierney, J. E., Zhu, J., King, J., Malevich, S. B., Hakim, G. J., and Poulsen, C. J.: Glacial cooling and climate
735 sensitivity revisited, *Nature*, 584, 569+, 10.1038/s41586-020-2617-x, 2020.

736 van Bree, L. G. J., Peterse, F., Baxter, A. J., De Crop, W., van Grinsven, S., Villanueva, L., Verschuren, D., and
737 Sinninghe Damsté, J. S.: Seasonal variability and sources of in situ brGDGT production in a permanently stratified
738 African crater lake, *Biogeosciences*, 17, 5443-5463, 10.5194/bg-17-5443-2020, 2020.

739 Wang, G., Wang, Y., Wei, Z., He, W., Ma, X., and Zhang, T.: Reconstruction of temperature and precipitation
740 spanning the past 28 kyr based on branched tetraether lipids from Qionghai Lake, southwestern China,
741 *Palaeogeography Palaeoclimatology Palaeoecology*, 562, 10.1016/j.palaeo.2020.110094, 2021a.

742 Wang, H., An, Z., Lu, H., Zhao, Z., and Liu, W.: Calibrating bacterial tetraether distributions towards in situ soil
743 temperature and application to a loess-paleosol sequence, *Quaternary Science Reviews*, 231,
744 10.1016/j.quascirev.2020.106172, 2020.

745 Wang, H., Chen, W., Zhao, H., Cao, Y., Hu, J., Zhao, Z., Cai, Z., Wu, S., Liu, Z., and Liu, W.: Biomarker-based
746 quantitative constraints on maximal soil-derived brGDGTs in modern lake sediments, *Earth and Planetary Science
747 Letters*, 602, 10.1016/j.epsl.2022.117947, 2023.

748 Wang, H., Liu, W., He, Y., Zhou, A., Zhao, H., Liu, H., Cao, Y., Hu, J., Meng, B., Jiang, J., Kolpakova, M.,
749 Krivonogov, S., and Liu, Z.: Salinity-controlled isomerization of lacustrine brGDGTs impacts the associated
750 MBT5ME' terrestrial temperature index, *Geochimica et Cosmochimica Acta*, 305, 33-48,
751 10.1016/j.gca.2021.05.004, 2021b.

752 Wang, M., Liang, J., Hou, J., and Hu, L.: Distribution of GDGTs in lake surface sediments on the Tibetan Plateau
753 and its influencing factors, *Science China Earth Sciences*, 59, 961-974, 10.1007/s11430-015-5214-3, 2016.

754 Wang, M. D., Hou, J. Z., Duan, Y. W., Chen, J. H., Li, X. M., He, Y., Lee, S. Y., and Chen, F. H.: Internal feedbacks
755 forced Middle Holocene cooling on the Qinghai-Tibetan Plateau, *Boreas*, 10.1111/bor.12531, 2021c.

756 Wang, N., Liu, L., Hou, X., Zhang, Y., Wei, H., and Cao, X.: Palynological evidence reveals an arid early Holocene
757 for the northeast Tibetan Plateau, *Climate of the Past*, 18, 2381-2399, 10.5194/cp-18-2381-2022, 2022.

758 Weber, Y., De Jonge, C., Rijpstra, W. I. C., Hopmans, E. C., Stadnitskaia, A., Schubert, C. J., Lehmann, M. F.,
759 Sinninghe Damsté, J. S., and Niemann, H.: Identification and carbon isotope composition of a novel branched
760 GDGT isomer in lake sediments: Evidence for lacustrine branched GDGT production, *Geochimica et*
761 *Cosmochimica Acta*, 154, 118-129, 10.1016/j.gca.2015.01.032, 2015.

762 Weber, Y., Sinninghe Damste, J. S., Zopfi, J., De Jonge, C., Gilli, A., Schubert, C. J., Lepori, F., Lehmann, M. F.,
763 and Niemann, H.: Redox-dependent niche differentiation provides evidence for multiple bacterial sources of
764 glycerol tetraether lipids in lakes, *Proc Natl Acad Sci U S A*, 115, 10926-10931, 10.1073/pnas.1805186115, 2018.

765 Weijers, J. W. H., Schouten, S., van den Donker, J. C., Hopmans, E. C., and Sinninghe Damsté, J. S.:
766 Environmental controls on bacterial tetraether membrane lipid distribution in soils, *Geochimica et Cosmochimica*
767 *Acta*, 71, 703-713, 10.1016/j.gca.2006.10.003, 2007.

768 Woltering, M., Werne, J. P., Kish, J. L., Hicks, R., Sinninghe Damsté, J. S., and Schouten, S.: Vertical and temporal
769 variability in concentration and distribution of thaumarchaeotal tetraether lipids in Lake Superior and the
770 implications for the application of the TEX86 temperature proxy, *Geochimica et Cosmochimica Acta*, 87, 136-
771 153, 10.1016/j.gca.2012.03.024, 2012.

772 Wu, D., Chen, X., Lv, F., Brenner, M., Curtis, J., Zhou, A., Chen, J., Abbott, M., Yu, J., and Chen, F.: Decoupled
773 early Holocene summer temperature and monsoon precipitation in southwest China, *Quaternary Science Reviews*,
774 193, 54-67, 10.1016/j.quascirev.2018.05.038, 2018.

775 Wu, J., Yang, H., Pancost, R. D., Naafs, B. D. A., Qian, S., Dang, X., Sun, H., Pei, H., Wang, R., Zhao, S., and
776 Xie, S.: Variations in dissolved O₂ in a Chinese lake drive changes in microbial communities and impact
777 sedimentary GDGT distributions, *Chemical Geology*, 579, 10.1016/j.chemgeo.2021.120348, 2021.

778 Yan, T., Zhao, C., Yan, H., Shi, G., Sun, X., Zhang, C., Feng, X., and Leng, C.: Elevational differences in Holocene
779 thermal maximum revealed by quantitative temperature reconstructions at ~30° N on eastern Tibetan Plateau,
780 *Palaeogeography, Palaeoclimatology, Palaeoecology*, 570, 110364, 10.1016/j.palaeo.2021.110364, 2021.

781 Yao, T., Bolch, T., Chen, D., Gao, J., Immerzeel, W., Piao, S., Su, F., Thompson, L., Wada, Y., Wang, L., Wang,
782 T., Wu, G., Xu, B., Yang, W., Zhang, G., and Zhao, P.: The imbalance of the Asian water tower, *Nature Reviews*
783 *Earth & Environment*, 3, 618-632, 10.1038/s43017-022-00299-4, 2022.

784 Zhang, C., Zhao, C., Yu, S.-Y., Yang, X., Cheng, J., Zhang, X., Xue, B., Shen, J., and Chen, F.: Seasonal imprint
785 of Holocene temperature reconstruction on the Tibetan Plateau, *Earth-Science Reviews*, 226, 103927,
786 10.1016/j.earscirev.2022.103927, 2022a.

787 Zhang, E., Chang, J., Shulmeister, J., Langdon, P., Sun, W., Cao, Y., Yang, X., and Shen, J.: Summer temperature
788 fluctuations in Southwestern China during the end of the LGM and the last deglaciation, *Earth and Planetary*
789 *Science Letters*, 509, 78-87, 10.1016/j.epsl.2018.12.024, 2019a.

790 Zhang, E., Chang, J., Cao, Y., Sun, W., Shulmeister, J., Tang, H., Langdon, P. G., Yang, X., and Shen, J.: Holocene
791 high-resolution quantitative summer temperature reconstruction based on subfossil chironomids from the

792 southeast margin of the Qinghai-Tibetan Plateau, *Quaternary Science Reviews*, 165, 1-12,
793 10.1016/j.quascirev.2017.04.008, 2017.

794 Zhang, G., Luo, W., Chen, W., and Zheng, G.: A robust but variable lake expansion on the Tibetan Plateau, *Science*
795 *Bulletin*, 64, 1306-1309, 10.1016/j.scib.2019.07.018, 2019b.

796 Zhang, W., Wu, H., Cheng, J., Geng, J., Li, Q., Sun, Y., Yu, Y., Lu, H., and Guo, Z.: Holocene seasonal temperature
797 evolution and spatial variability over the Northern Hemisphere landmass, *Nat Commun*, 13, 5334,
798 10.1038/s41467-022-33107-0, 2022b.

799 Zhao, B., Castaneda, I. S., Bradley, R. S., Salacup, J. M., de Wet, G. A., Daniels, W. C., and Schneider, T.:
800 Development of an in situ branched GDGT calibration in Lake 578, southern Greenland, *Organic Geochemistry*,
801 152, 10.1016/j.orggeochem.2020.104168, 2021a.

802 Zhao, C., Liu, Z. H., Rohling, E. J., Yu, Z. C., Liu, W. G., He, Y. X., Zhao, Y., and Chen, F. H.: Holocene
803 temperature fluctuations in the northern Tibetan Plateau, *Quaternary Research*, 80, 55-65,
804 10.1016/j.yqres.2013.05.001, 2013.

805 Zhao, C., Rohling, E. J., Liu, Z., Yang, X., Zhang, E., Cheng, J., Liu, Z., An, Z., Yang, X., Feng, X., Sun, X.,
806 Zhang, C., Yan, T., Long, H., Yan, H., Yu, Z., Liu, W., Yu, S.-Y., and Shen, J.: Possible obliquity-forced warmth
807 in southern Asia during the last glacial stage, *Science Bulletin*, 66, 1136-1145, 10.1016/j.scib.2020.11.016, 2021b.

808 Zheng, Y., Li, Q., Wang, Z., Naafs, B. D. A., Yu, X., and Pancost, R. D.: Peatland GDGT records of Holocene
809 climatic and biogeochemical responses to the Asian Monsoon, *Organic Geochemistry*, 87, 86-95,
810 10.1016/j.orggeochem.2015.07.012, 2015.

811 Zhou, W., Yu, S.-Y., Burr, G. S., Kukla, G. J., Jull, A. J. T., Xian, F., Xiao, J., Colman, S. M., Yu, H., Liu, Z., and
812 Kong, X.: Postglacial changes in the Asian summer monsoon system: a pollen record from the eastern margin of
813 the Tibetan Plateau, *Boreas*, 39, 528-539, 10.1111/j.1502-3885.2010.00150.x, 2010.

814 Zielinski, G. A. and Mershon, G. R.: Paleoenvironmental implications of the insoluble microparticle record in the
815 GISP2 (Greenland) ice core during the rapidly changing climate of the Pleistocene-Holocene transition,
816 *Geological Society of America Bulletin*, 109, 547-559, 10.1130/0016-7606(1997)109<0547:piotim>2.3.co;2,
817 1997.

818

819